The Robust Lamina Cribrosa Vasculature: Perfusion and Oxygenation Under Elevated Intraocular Pressure

Yuankai Lu,[1] Yi Hua,[1–3] Bingrui Wang,[1] Fuqiang Zhong,[1] Andrew Theophanous,[4] Shaharoz Tahir,[4] Po-Yi Lee,[1,4] and Ian A. Sigal[1,4]

[1]Department of Ophthalmology, University of Pittsburgh, Pittsburgh, Pennsylvania, United States
[2]Department of Biomedical Engineering, University of Mississippi, Mississippi, United States
[3]Department of Mechanical Engineering, University of Mississippi, Mississippi, United States
[4]Department of Bioengineering, University of Pittsburgh, Pittsburgh, Pennsylvania, United States

Correspondence: Ian A. Sigal, Department of Ophthalmology, University of Pittsburgh, UPMC Mercy Pavilion, 1622 Locust St. Rm. 7.382, Pittsburgh, PA 15219, USA; ian@ocularbiomechanics.com.

Received: November 20, 2023
Accepted: March 21, 2024
Published: May 1, 2024

Citation: Lu Y, Hua Y, Wang B, et al. The robust lamina cribrosa vasculature: Perfusion and oxygenation under elevated intraocular pressure. *Invest Ophthalmol Vis Sci.* 2024;65(5):1. https://doi.org/10.1167/iovs.65.5.1

Purpose. Elevated intraocular pressure (IOP) is thought to cause lamina cribrosa (LC) blood vessel distortions and potentially collapse, adversely affecting LC hemodynamics, reducing oxygenation, and triggering, or contributing to, glaucomatous neuropathy. We assessed the robustness of LC perfusion and oxygenation to vessel collapses.

Methods. From histology, we reconstructed three-dimensional eye-specific LC vessel networks of two healthy monkey eyes. We used numerical simulations to estimate LC perfusion and from this the oxygenation. We then evaluated the effects of collapsing a fraction of LC vessels (0%–36%). The collapsed vessels were selected through three scenarios: stochastic (collapse randomly), systematic (collapse strictly by the magnitude of local experimentally determined IOP-induced compression), and mixed (a combination of stochastic and systematic).

Results. LC blood flow decreased linearly as vessels collapsed—faster for stochastic and mixed scenarios and slower for the systematic one. LC regions suffering severe hypoxia (oxygen <8 mm Hg) increased proportionally to the collapsed vessels in the systematic scenario. For the stochastic and mixed scenarios, severe hypoxia did not occur until 15% of vessels collapsed. Some LC regions had higher perfusion and oxygenation as vessels collapsed elsewhere. Some severely hypoxic regions maintained normal blood flow. Results were equivalent for both networks and patterns of experimental IOP-induced compression.

Conclusions. LC blood flow was sensitive to distributed vessel collapses (stochastic and mixed) and moderately vulnerable to clustered collapses (systematic). Conversely, LC oxygenation was robust to distributed vessel collapses and sensitive to clustered collapses. Locally normal flow does not imply adequate oxygenation. The actual nature of IOP-induced vessel collapse remains unknown.

Keywords: lamina cribrosa, perfusion, oxygenation, intraocular pressure, hypoxia

Glaucoma is a leading cause of blindness worldwide. The disease is characterized by progressive degeneration of retinal ganglion cells (RGCs) and their axons.[1,2] In early glaucoma, the axon damage is believed to start within the lamina cribrosa (LC) region of the optic nerve head (ONH).[3,4] The highly connected and complex vascular network of the LC provides nutritional support and oxygen to the RGC axons.[5–9] Although the mechanisms of axon damage within the LC remain unclear,[10–15] it has long been thought that a primary contributor is an insufficient oxygen supply within the ONH due to reduced blood perfusion.[16–19] Elevated intraocular pressure (IOP), one of the top risk factors for glaucoma, may contribute to this process.[11,20] Elevated IOP can induce LC deformations, leading to the distortion and potentially collapse of vasculature.[10,12,21–23] Distortion and collapse of the vessels, in turn, would adversely affect blood flow through the LC, compromising the oxygen supply.[11,20,24] The effects of a reduced oxygen supply on the LC neural tissues will depend on the strength of the insult.[25–28] A mild decrease in oxygenation may trigger a different response than a severe level of hypoxia.[26,29,30] A comprehensive analysis of the link between the blood/oxygen supply and the potential vessel collapse resulting from IOP elevation will help understand the development of glaucoma.

Over the last several years, light-based imaging tools, primarily optical coherence tomography angiography (OCTA), have made tremendous advances in resolution and now even allow measuring levels of blood oxygenation.[31–34] The techniques, however, still cannot provide the level of detail in the deep tissues of the ONH to visualize and analyze LC vessels and blood flow.[35] Sound-based techniques, although capable of deeper penetration, lack the necessary resolution to discern the small vessels of the ONH.[36] Magnetic resonance imaging–based techniques also have excellent penetration and the ability to provide

detailed information on chemical composition, but the resolution, spatial and temporal, is insufficient for the LC.[37] Laser speckle flowgraphy can measure blood flow on the ONH,[38] but it lacks resolution along the depth direction. Hence, there are currently no experimental tools with the temporal and three-dimensional (3D) spatial resolutions and depth penetration necessary to measure blood flow and oxygenation within the ONH. Therefore, theoretical modeling and numerical simulation have been used for evaluating LC hemodynamics (blood flow perfusion rate) and oxygenation.[11,12,20,39] These models, although insightful, are limited by the simplified and generic LC vasculature assumption. To address this limitation, we recently demonstrated that it is possible to reconstruct[40] and then use for hemodynamics and oxygenation simulation[41] a model of the complex eye-specific highly interconnected 3D vascular network of the LC region. A parametric analysis based on the eye-specific model showed that conditions that reduce vessel diameter, such as vessel compression due to elevated IOP or gaze-induced tissue deformation, may particularly contribute to decrease LC oxygen concentration.[41]

Our goal for this study was to evaluate the robustness of the LC vasculature in terms of its ability to preserve blood perfusion and oxygenation in the face of IOP-related vessel collapses. We leveraged our recently reported model reconstruction and simulation techniques to reconstruct the vascular networks of two monkey ONHs.[40,41] For the models as reconstructed (baselines), we first calculated the perfusion (blood flow) for all the network and from this the oxygen pressure. We then evaluated how the perfusion and oxygenation were affected by a progressively increasing number of collapsed vessels, from none at baseline up to 36% of the network vessel segments. It is unclear from experimental studies when vessel collapse occurs, and vessels may only distort without full collapse. We considered collapse as a worst-case scenario that is useful to evaluate the robustness. To select the vessels for collapse we used three scenarios: a stochastic approach, in which the vessels collapsed were selected randomly; a systematic approach, in which the vessels were collapsed in order according to an experimentally defined map of IOP-induced tissue distortion (vessels in locations with the largest compression collapse first); and a mixed approach. For each model, we determined the changes in blood perfusion and oxygenation compared with the baseline. We then determined the regions with mild or severe hypoxia. To avoid potential biases in the scenarios involving stochastic decisions, we repeated the process 50 times. We repeated the process for two sets of experimental IOP-related deformations. The process described above required a very large number of simulations. For efficiency, we implemented recently developed techniques that allow much faster modeling of flow and oxygen/nutrient distribution in networks.[42] The effects of the vascular collapse on the blood flow and oxygenation within the LC thus give an indication of the robustness of the LC vasculature.

Methods

An overview of the general procedure is provided in Figure 1. The steps are described in more detail in the subsections below.

Vessel Reconstruction

We followed the process reported before.[40,43] In accordance with University of Pittsburgh's Institutional Animal Care and Use Committee approval and following National Institutes of Health guidelines and the ARVO Statement for the Use of Animals in Ophthalmic and Vision Research, we prepared two healthy female rhesus macaque monkeys for vessel labeling. The anterior chambers of the eyes were cannulated to maintain IOP at 5 mm Hg throughout the experiment. Dil, a lipophilic carbocyanine dye, was used to label the vessels in the eye. We perfused aqueous 100 mL Dil solution into each carotid artery and then perfused 100 mL formalin into each carotid artery to fix the eye.

The ONH and surrounding sclera were then processed, sectioned, and imaged using fluorescence microscopy (FM) and polarized light microscopy (PLM). Stacks of sequential FM and PLM images were aligned and registered using Avizo 9.1 software. After registration, the FM images were segmented and skeletonized to create a 3D reconstruction of the ONH vasculature.

As in our previous study,[41] we reconstructed the vessels within the scleral canal and immediate periphery. The vessels in the canal included the whole LC region, and vessels in the prelaminar and retrolaminar regions (Fig. 2). This ensured that the 3D LC network was fully enclosed within the region reconstructed, without any of the LC vessels directly in the model boundary. The LC region was defined based on the presence of collagen beams in the PLM.[40,43] With the LC region defined, we then identified the vessel segments within the region as LC vessels. Because the label perfusion was done postmortem, we could not ensure that the vessel diameters in the sections were truly representative of the in vivo condition. Hence, we assumed a uniform capillary diameter of 8 µm.[44]

Hemodynamic and Oxygenation Model

Hemodynamic Modeling. The process we used to complete LC vessel network reconstruction and how these were turned into numerical models for hemodynamics have been described elsewhere.[41] For the actual simulations of blood flow within the ONH vasculature, we followed the approach described in Lu et al.[42] The vasculature was simulated as a network system, which was represented as a set of interconnected capillary elements. Due to the low Reynolds number in capillaries, the blood flow within a capillary can be approximately by the Poiseuille flow:

$$Q = \frac{\pi r^4}{8\mu L}\Delta P$$

where Q is the volume flow rate, r is the vessel radius, L is the vessel length, µ is the blood viscosity, and ΔP is the pressure drop along the vessel.

Pressure boundary conditions were applied to simulate the physiological blood supply for ONH. Specifically, the model boundaries were divided into four regions for assigning the blood pressure conditions that drive the blood flow throughout the vascular network (Fig. 2). We set arteriole inlet pressure to 50 mm Hg at the periphery to simulate blood inflow from the circle of Zinn–Haller, a venule outlet pressure of 15 mm Hg at the central retinal vein for drainage, a pressure of 20 mm Hg at the anterior ONH, and a pressure of 16 mm Hg at the posterior ONH.

Investigative Ophthalmology & Visual Science

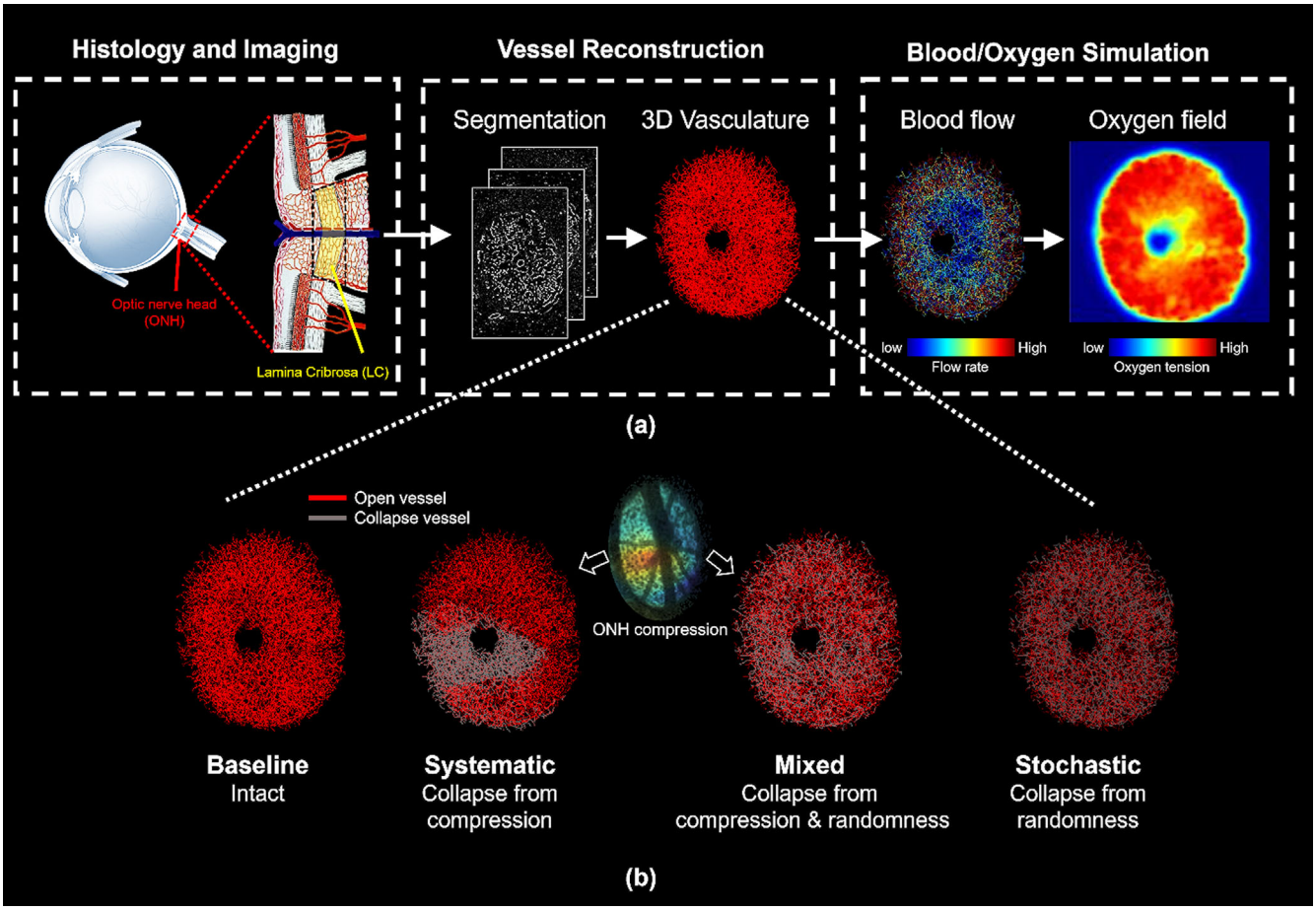

Figure 1. (**a**) The general workflow process. Two vasculatures of normal monkey ONHs were perfusion-labeled and imaged as histological sections. The images were aligned and stacked to form a volume. We then reconstructed the eye-specific vasculatures of monkey ONHs using image segmentation and skeletonization techniques. The vessel networks were converted into numerical models and boundary conditions applied. Simulations were then performed to obtain first the blood flow and from this the oxygen field within the ONHs. (**b**) Baseline vasculature and compromised vasculature. Three different collapse scenarios (systematic, mixed, and stochastic) were applied to the baseline vasculature to generate the collapsed ones.

Oxygenation Modeling. Our ONH oxygenation simulation was based on the blood flow field, simulating the transport of oxygen from microvascular networks to tissues, as reported before.[45] The physical principles of oxygen transport are well established, including diffusion within tissue and convection within vessels. The oxygen diffusion and consumption in tissue can be described by:

$$D\alpha\Delta P = M(P),\ M(P) = M_0P/(P_0 + P)$$

where D is the oxygen diffusion coefficient, α is the oxygen solubility coefficient, and P is the tissue oxygen partial pressure. The oxygen consumption rate, $M(P)$, can be estimated by Michaelis–Menten enzyme kinetics, where M_0 represents demand and P_0 is the oxygen partial pressure at half-maximal consumption. In this study, M_0 was assumed to be uniform throughout the LC.

The oxygen flux in blood vessels satisfied the following equation:

$$f(P_b) = Q\left(H_DC_0S(P_b) + \alpha_{eff}P_b\right)$$

where H_D is the hematocrit, C_0 is the concentration of hemoglobin-bound oxygen in a fully saturated red blood cell, P_b is the blood oxygen partial pressure (mm Hg), $S(P_b)$ is the oxygen–hemoglobin saturation as determined by the Hill equation, and α_{eff} is the effective solubility of oxygen in plasma. All parameters are listed in the Table.

We applied a fast and efficient method to simulate the convective and diffusive oxygen transport.[42] The ONH oxygen field within the LC was used to determine the regions of the LC suffering hypoxia.

Vessel Collapse Scenarios

To simulate the potential challenge to the vascular network, we speculated that, under pathological IOP levels or even some physiological ones in sensitive eyes, a fraction of the vessel in ONH would distort and potentially collapse, occluding blood flow.[46,47] The fraction of occluded vessels (R_c) was defined as the number of collapsed vessels divided by the number of total vessels. To simulate vascular networks facing various levels of challenge, the collapse ratio was systematically varied from 0% to 36% in increments of 2%. In addition to a collapse ratio, we still needed to specify a collapse mechanism to determine which vessel would experience collapse. To the best of our knowledge, there is no direct experimental evidence of how the vessels collapse. Generally, it is believed that elevated IOP is a major

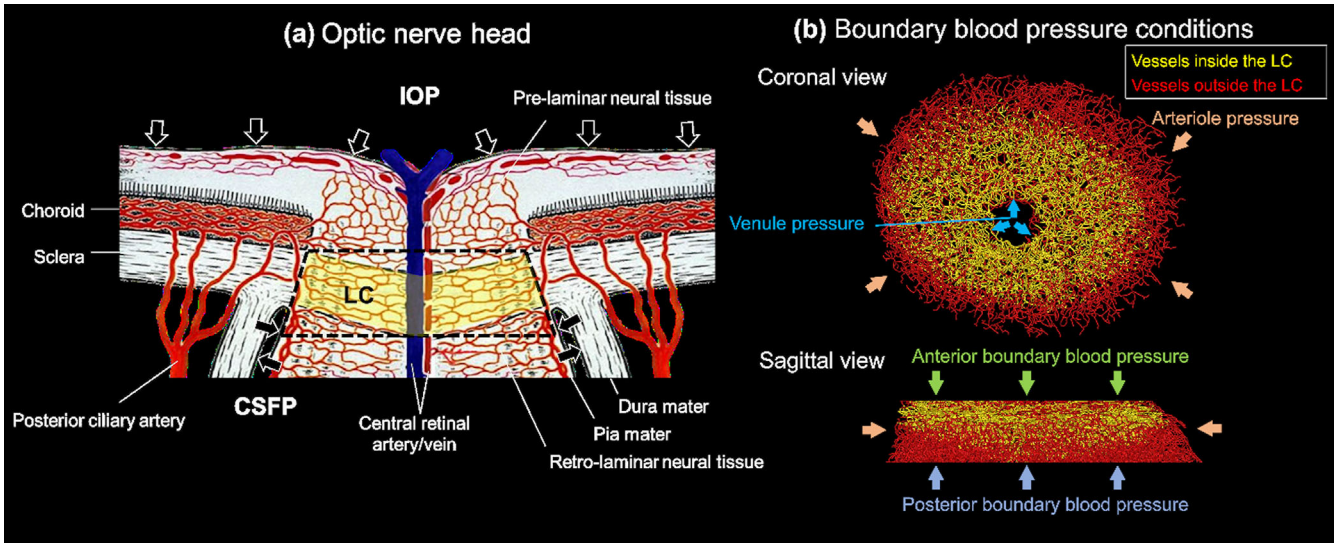

Figure 2. (**a**) Schematic of the ONH (adapted from Hua et al.[41]). The reconstructed network included the vessels in a region encompassing the LC and pre- and retrolaminar tissues within the scleral canal, as well as some vessels in the periphery. The model was thus delimited in the periphery by the connective tissues of the sclera and/or pia mater and by the central retinal artery and vein in the center. The *black dashed lines* represent the model boundaries, which extend within the canal beyond the LC region (*yellow*). (**b**) Four blood pressure boundary conditions were assigned at the peripheral, central, anterior, and posterior boundaries of the model.

Table. Parameters Used in Hemodynamic and Oxygenation Simulations

Parameter	Value	Ref.
Hemodynamic		
Vessel diameter	8 µm	Hua et al.[41]
Arteriole pressure	50 mm Hg	Hua et al.[41]
Venule pressure	15 mm Hg	Hua et al.[41]
Anterior blood pressure	20 mm Hg	Hua et al.[41]
Posterior blood pressure	16 mm Hg	Hua et al.[41]
Oxygenation		
Oxygen diffusion coefficient ($D\alpha$)	6×10^{-10} mLO_2/cm/s/mm Hg	Secomb et al.[45]
Effective oxygen solubility (α_{eff})	3.1×10^{-5} mLO_2/mL/mm Hg	Chuangsuwanich et al.,[12] Secomb et al.[45]
Consumption rate (M_0)	5×10^{-4} mLO_2/mL/s	Hua et al.[41]
Oxygenation at half-maximal consumption (P_0)	10.5 mm Hg	Secomb et al.[45]
Maximal RBC oxygen concentration (C_0)	0.5 mLO_2/mL	Chuangsuwanich et al.,[12] Secomb et al.[45]

contributing factor,[10,48,49] but potentially not the only one. Other collapse factors could include the diameter of the vessel and interactions with the LC collagenous beam.[5,43] It is also possible that other systemic conditions could affect vessel collapse, such as diabetes and inflammation.[50,51] Finally, given that the LC and optic nerve are part of the central nervous system, autoregulation may play a role.[52] Although autoregulation is expected to be minimal within the LC,[53–55] it may still affect the periphery. Therefore, we modeled the vascular collapse scenarios as an IOP-driven process (systematic), IOP-independent process (stochastic), or a combination of them (mixed). The central retinal vein and artery were not included when selecting which blood vessels collapse. Further details regarding these scenarios are provided in the Appendix.

Systematic Collapse Scenario. In this scenario, vascular collapse was modeled as a sequential systematic process and was entirely determined by IOP-induced tissue deformation. Specifically, blood vessels collapsed in series, starting with vessels experiencing the highest magnitude of local tissue compression, followed by the vessels with second largest compression, and so on and so forth. The collapse process continued until the proportion of collapsed vessel reached our setting R_c. This process is entirely systematic and deterministic; therefore, only one simulation is required for each case at each occluded ratio. Note that four cases were considered: two LC vessel networks, each one subjected to maps of experimentally measured IOP-induced deformations from two eyes.

Stochastic Collapse Scenario. In this scenario, the vascular collapse was modeled as a completely random process, where each vessel had a uniform likelihood of collapsing. This randomness can partially be attributed to variations in the material properties of the vessels and their individual susceptibility to collapse during IOP elevation, as discussed above. Pathological and physiological conditions that are independent of IOP can also contribute to vascular collapse; thus, the randomness represents an extreme of this scenario. To account for the randomness, we performed 50 simulations for each case, which meant 50

totally independent sequences of collapsed vessels from 0% to 36%.

Mixed Collapse Scenario. In this scenario, the vascular collapse was modeled as a mix of fully systematic and fully stochastic processes, where each vessel collapsed in weighted likelihood (the probability of collapse is proportional to the IOP-induced compression). This scenario is a combination of the systematic and stochastic scenarios as described above and was intended to capture a situation where vessel collapse is more likely due to higher local IOP-induced tissue compression but where other complex factors, including individual vessel susceptibility to collapse due to variations in material properties, may increase or decrease the risk. Specifically, we used a weighted collapse probability for each vessel, where the probability is proportional to the surrounding tissue compression. We refer readers to the Appendix for a detailed mathematical description of the collapse probability. Again, to account for the stochastic nature of the process, we repeated the simulations 50 times.

Summary. We reconstructed two eye-specific vessel networks. For each vessel network, we considered 18 collapse ratios, ranging from 2% to 36% with an increment of 2%. Therefore, there were 36 baseline models for each vessel collapse scenario. In the stochastic scenario, we randomly selected the collapsed vessels 50 times for each model, resulting in a total of 1800 simulations (36 × 50). In the systematic scenario, a deterministic approach, we applied ONH deformations from two experimental datasets for each model, resulting in a total of 72 simulations (36 × 2). In the mixed scenario, we randomly selected the collapsed vessels 50 times for each model and applied ONH deformations from two experimental datasets, resulting in a total of 3600 simulations (36 × 50 × 2). Thus, the total number of simulations was 5472: 1800 stochastic + 72 systematic + 3600 mixed.

Tissue Compression and Vessel Collapse

The deformation of blood vessels is influenced by various factors, including the surrounding tissue strain, compliance of the vessel wall, and blood pressure.[56] In this study, we simplified the estimation of vessel collapse by focusing on the IOP-induced ONH tissue compression. Specifically, we calculated the average tissue compression at the vessel wall to assess the probability of vessel collapse. Vessels experiencing significant compression had a higher risk of collapse in both systematic and mixed scenarios. To account for variations among different eyes, we employed two experimental IOP-induced ONH strain data in our sequential and mixed collapse scenarios. The experimental compression maps were obtained as described elsewhere.[57] Briefly, optical coherence tomography (OCT) volume scans were obtained of the ONH of a monkey while IOP was manometrically controlled. Images obtained at 10 and 40 mm Hg were analyzed using a digital volume correlation (DVC) algorithm. Data from two monkey eyes were used. The ONH compressions and vascular networks originate from different eyes. Hence, we translated and rotated the deformation field to register it with the central retinal artery and vein and align the temporal–nasal–superior–inferior axes across both samples. We then used a linear interpolation method to evaluate the average tissue compression at the surface of each vessel.

Robustness Analysis

The hemodynamics and oxygenation simulations were done for the full reconstructed ONH vasculature, which contains the LC region. We then conducted the robustness analysis focusing on the LC region. The quantifications in the sections below thus correspond to the vasculature within the LC region only.

Blood Perfusion. For the three collapse scenarios, we investigated the effects of the collapse ratio on the total blood perfusion rate in the LC region. The perfusion rate (nL/min) was defined as the cumulative sum of all inlet flow and was also equal to the sum of all outlet flow. Blood perfusion defined in this way has been shown to play a crucial role in maintaining normal tissue physiology and serves as an important clinical indicator for microcirculation function.[58]

Oxygen Supply. Tissue hypoxia, characterized by reduced tissue oxygenation, is generally a consequence of structurally and functionally disturbed microcirculation.[28,59] We used the estimated size of the hypoxia region as a surrogate measure of potential damage caused by various vascular collapse scenarios and, through this, as an indicator of LC robustness. The hypoxia-driven pathological processes involve various complex biochemical mechanisms and vary significantly across different tissues.[26,28,60] In general, a normal oxygen supply ensures physiological cellular activity. As the oxygen pressure decreases, the risk of damage to the tissues increases. If oxygen partial pressure is sufficiently low, irreversible damage such as tissue necrosis may occur.[29] To distinguish among the potential levels of hypoxia, we classified the tissues into three levels based on the local oxygen partial pressure:

1. Normoxia (>38 mm Hg)—Normal cellular activity and metabolism.
2. Mild hypoxia (8~38 mm Hg)—Normal physiological responses to hypoxia occur, returning oxygen partial pressure to a normal level; if sustained chronically, mild hypoxia may contribute to neural tissue damage.
3. Severe hypoxia (<8 mm Hg)—Tissue necrosis, irreversible damage.

The rationale for the oxygen tension range is as follows: 8 mm Hg (~1% oxygen) has been consistently used as a threshold for severe hypoxia in neural tissues.[25,61,62] Tissue normoxia, however, varies widely, from 20 mm Hg to 50 mm Hg and is difficult to measure under in vivo ONH conditions.[26,59,61,63] Considering the hypoxia-sensitive neural cells in the LC region, we analyzed precedents set in existing literature in the normal ONH and cerebral cortex.[25–28] We settled on a threshold of 38 mm Hg (~5% oxygen) for tissue normoxia, as used in McKeown et al.[29] The mild hypoxia was then selected as the intermediate state between normoxia and severe hypoxia.

We assessed the volumetric proportions of these three types of regions. Normoxia regions represented regions with an adequate oxygen supply. All of the LC was under normoxia at normal IOP. The mild and severe hypoxia regions, linked to potential damage caused by LC vessel collapse, were primarily utilized to evaluate LC oxygenation robustness.

Spatial Association Among Hemodynamics, Oxygenation, and ONH Compression. An important question emerged from the analysis of blood perfusion and oxygen supply: Are the reductions in perfusion and oxygenation directly linked to the local mechanical stress

induced by IOP? To address this, we conducted a qualitative spatial analysis of ONH hemodynamics, oxygenation, and compression. Specifically, we compared the distribution of collapsed vessels, blood flow, and oxygen fields at the same collapse ratio.

Results

The two vascular network structures utilized in the simulation are shown in Figure 3. Figure 4 shows the two tissue compression fields employed for the systematic/mixed collapse scenarios. Note that these fields were derived from the eyes of different monkeys than the networks of Figure 3. The two compression maps were applied to both eyes in the following analysis.

Blood Perfusion

The results of blood perfusion quantification for the three collapse scenarios are shown in Figure 5, along with two illustrations of the vessel networks colored by blood flow magnitude and histogram for inlet/outlet flow. Similar outcomes were observed for the two vascular networks and despite differences in ONH compressions.

Oxygen Supply

Figure 6 presents normoxia/hypoxia regions for various vessel collapse models and spatial oxygen field distributions and histograms for two specific collapse models. The tissue fraction was assessed based on the LC region, with a voxel size of $20 \times 20 \times 20\ \mu m^3$. The two eyes had distinct oxygen fields, with different sensitivities to the changes, but overall they still shared several characteristic responses. Generally, when the collapse ratio was relatively small (e.g., <10%), the severe hypoxia regions in the stochastic and mixed collapse models were negligible. Conversely, when the collapse ratio was relatively large (e.g., >30%), a large fraction of tissue suffered from severe hypoxia.

Spatial Association Among Hemodynamics, Oxygenation, and ONH Compression

Figure 7 shows the vessel networks colored by open/collapsed vessel or by blood flow and oxygen fields for an eye under the three collapse scenarios and for both compression maps. The side-by-side presentation simplifies qualitative interpretation of the spatial relationships between the outcomes. We observed that the spatial associations seem strong for the systematic scenario and moderate for the mixed one. This result is consistent with the previous results for oxygenation and perfusion. A quantitative comparison among the blood flow within vessels and the compression and oxygenation surrounding the vessels is shown in Figure 8. Figure 9 shows an illustration of blood flow and oxygenation across various depths of the LC.

Change in Oxygenation and Hemodynamics Under Various Collapse Ratios

Changes in the spatial distribution of hemodynamics and oxygenation under various collapse ratios are shown in Figure 10 and Figure 11. Our results showed that a few regions benefited from vessel collapse. Even though some vessels collapsed, there were still some areas that had better blood supply and oxygenation than the baseline.

Discussion

Our goal was to assess the robustness of the LC vasculature to vascular collapse that may result from elevated IOP. We evaluated both overall and local LC robustness in two

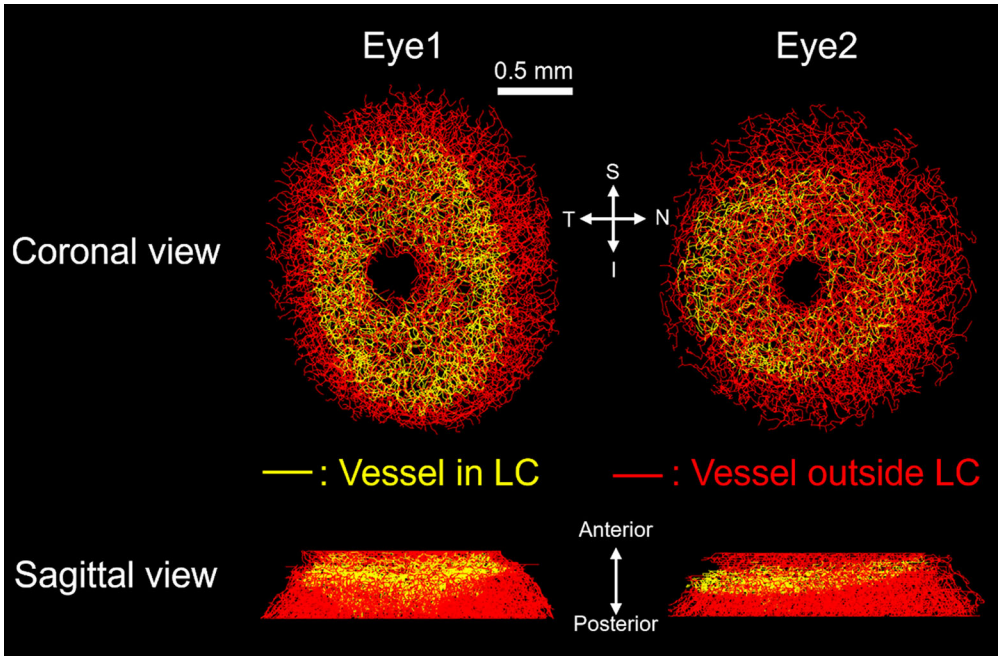

Figure 3. Coronal and sagittal views of the two 3D vascular networks. Both networks were reconstructed from the right eyes (OD) of healthy monkeys.

Investigative Ophthalmology & Visual Science

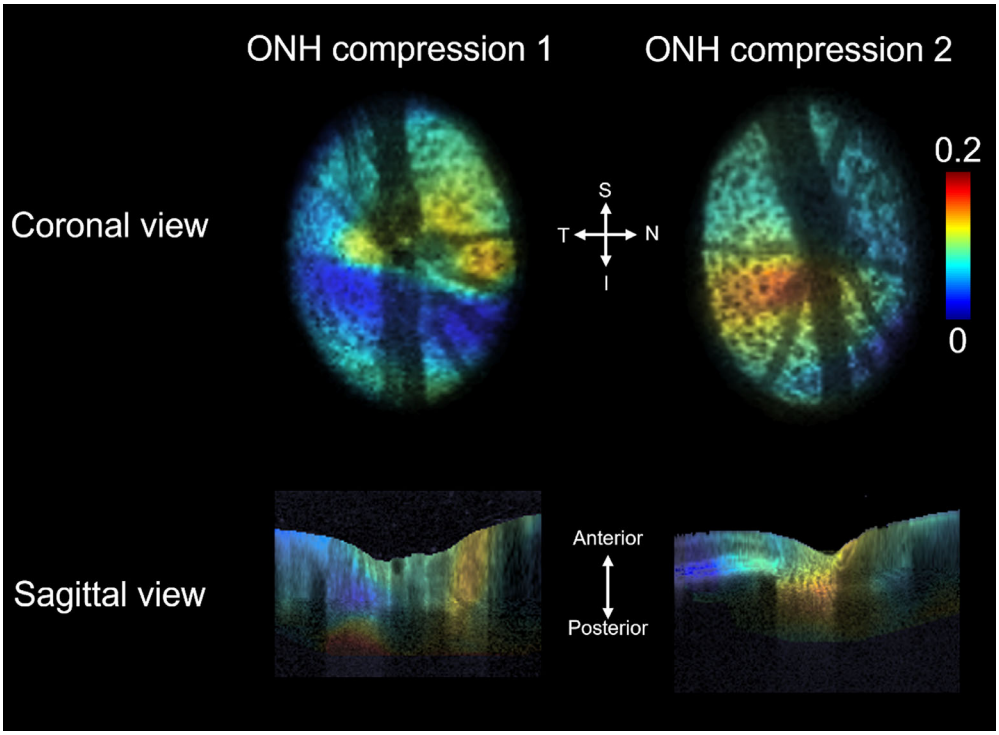

Figure 4. The two ONH compression fields used to predict vessel collapse. The fields were obtained by using image processing to measure tissue deformation induced by a change between a baseline (10 mm Hg) and elevated (40 mm Hg) IOPs. The deformations are shown in OD configuration. The OCT data and deformation analyses produce 3D information. Shown are cross-sections at the level of the LC colored according to the magnitude of IOP-induced compression. The two cases exhibited substantially different magnitudes and distributions of the compression.

specific outcomes: blood flow and oxygenation. Three main findings arise from this work. First, for overall blood flow, the LC was more robust to the clustered collapses of the systematic scenario than to the distributed vessel collapses of the stochastic and mixed scenarios. Overall blood flow decreased approximately linearly with collapse ratio in the three scenarios, but substantially faster for the stochastic and mixed scenarios and slower for the systematic one. Second, LC robustness was different for oxygenation than for blood flow. Overall LC oxygenation was more robust to the distributed vessel collapses of the stochastic and mixed scenarios and more sensitive to the clustered collapses of the systematic scenario. In the systematic scenario, LC regions suffering hypoxia (oxygen <8 mm Hg) increased proportionally to the collapsed vessels ratio, even for a few collapsed vessels. For the stochastic and mixed scenarios, severe hypoxia did not occur until 15% of the vessels had collapsed. Third, locally, there were small regions, or pockets, within the LC that had non-intuitive behaviors; for example, in some regions, blood perfusion and oxygenation increased as vessels collapsed elsewhere. Also, there were islands with normal blood flow but with very low oxygenation. Below we discuss each of the findings in detail.

For overall blood flow, the LC was more robust to the clustered collapses of the systematic scenario than to the distributed vessel collapses of the stochastic and mixed scenarios. The decreases in blood flow were approximately linear in all three scenarios, but the rates of decrease as a function of the collapse ratio were substantially faster for the stochastic and mixed scenarios than for the systematic one, which was roughly the same as the reference. This result was not surprising. It seems fairly clear that, as more vessels collapse, there are fewer vessels to carry blood through the network. Hence, each collapsed vessel causes a decrease in perfusion. What is not obvious for a network, especially one as complex as the one in the LC, is the specific relationship between the fraction of vessels collapsed and the decrease in blood flow. The ease with which blood can flow through a vessel network is sometimes measured by the "flow conductance."[64]

We believe that the explanation for the differences in LC robustness under the three scenarios is due to the distribution of the vessel collapses. In the stochastic and mixed scenarios, collapsed vessels are fairly independent, such that when one collapses the blood redistributes to adjacent vessels. Each collapse is thus independent of the previous ones. The independence decreases as the collapse ratio increases, explaining the curving of the lines in Figure 5. This leads to overall decreases in blood flow and a lower conductance. In contrast, in the systematic scenario, the collapsed vessels are clustered, and therefore the effects of vessel collapses are not independent. A collapsed vessel becomes insensitive to the collapse of adjacent vessels; hence, clustering of the collapses has more limited effects on the overall blood perfusion through the network than distributed vessel collapses.

There is substantial experimental evidence that blood perfusion in the ONH decreases with elevated IOP.[65–67] The explanation has been that elevated IOP distorts the tissues of the ONH, including compression and collapse of the LC vessels.[12,68] In this regard, our findings are consistent with

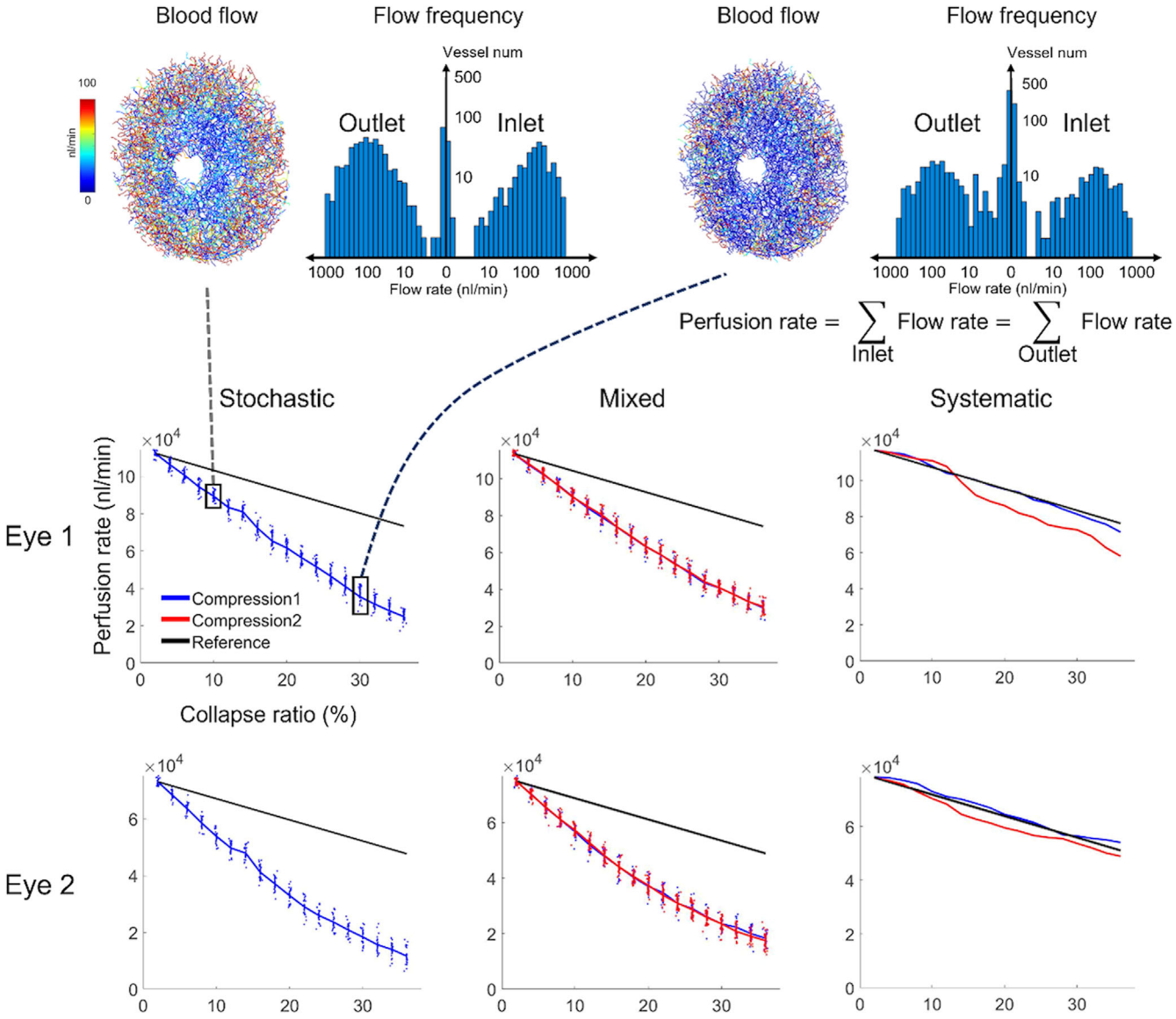

Figure 5. Perfusion in various vessel collapse scenarios, including two vasculatures with three collapse scenarios and two compression maps. (*Top row*) Detailed flow distribution and histograms of the same network under the same compression map 1, in the stochastic scenario for collapse ratios of 10% (*left*) and 30% (*right*). The total perfusion rate was defined as the sum of all inlet flow, which is equal to the sum of all outlet flow. Flow resulted from pressure differences between inlets and outlets; therefore, the total blood flow was not predetermined. Because blood flow rates vary greatly in scale, we used a logarithmic scale to display the distribution. Increases in the collapse ratio significantly reduced the number of high-flow vessels while increasing the number of low-flow vessels, resulting in a drop in perfusion rates. (*Middle and bottom rows*) The perfusion rates across the vessel collapse scenarios for both eyes. The columns correspond to the three scenarios. For the systematic case, there is only one case for each collapse ratio. For the stochastic and mixed scenarios, each data point represents one collapsed vessel network simulation. The points have some spread, indicating not only that the different potential stochastic paths for collapse lead to different results but also that the differences are small. The vertical range of the points is about the same as a 4% difference in collapse ratio. The spread increased slightly as the ratio of collapsed vessels increased. The *black reference lines* represent a 1:1 linear decrease in perfusion rate with respect to the collapse ratio. In most cases, perfusion flow decreases approximately linearly, with more pronounced reductions in the stochastic and mixed models. The overall effect of the collapse in the systematic scenario was a smaller loss of perfusion, with losses almost colinear with the reference line, than in the stochastic and mixed scenarios. This should be contrasted with the effects on the oxygen supply shown in Figure 6.

the literature. We are not aware, however, of studies quantifying the vessel collapse as a function of IOP or of measurements of changes in LC blood perfusion as vessels collapse, likely due to the lack of suitable experimental tools, which was one of the core motivations for our use of computational techniques.

LC robustness was different for oxygenation than for blood flow. Overall LC oxygenation was more robust to the distributed vessel collapses of the stochastic and mixed scenarios and more sensitive to the clustered collapses of the systematic scenario. In the systematic scenario, LC regions suffering hypoxia (oxygen <8 mm Hg) increased proportionally to the collapsed vessels ratio, even for a few collapsed vessels. For the stochastic and mixed scenarios severe hypoxia did not occur until 15% of the vessels had collapsed

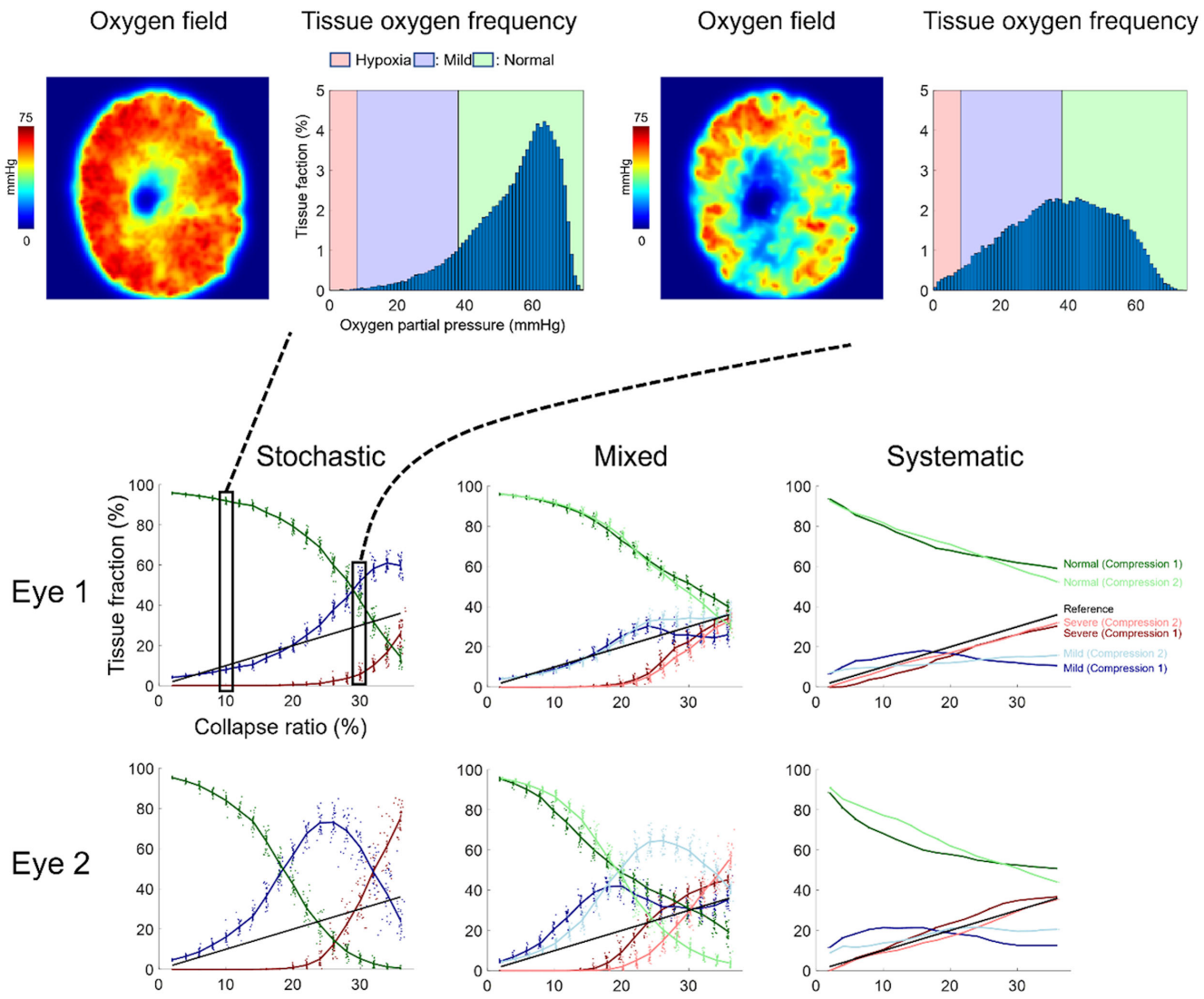

Figure 6. Quantitative analysis of the tissue fraction under normoxia, mild, or severe hypoxia for both vessel networks and under the various scenarios and compression maps. The two compression maps were applied to each eye in the following analysis. This figure is similar to Figure 5, but for the oxygen supply. (*Top row*) Illustration of the spatial distribution and histogram of oxygen field for two cases: the stochastic scenario with 10% and 30% collapse ratios. Tissues were categorized as normoxia, mild hypoxia, and severe hypoxia based on the local oxygenation levels. As expected, tissues had excellent perfusion at baseline without any severe hypoxia. As the collapse ratio increased, first the fraction of mild hypoxia increased and then the fraction of severe hypoxia. The case with 30% vessel collapse has about as much tissue under mild or severe hypoxia as under normoxia. (*Middle and bottom rows*) Plots of normoxia/hypoxia region size in various vessel collapse models. Each data point represents one collapsed vessel network model. The plots show the relationship between the percentage of tissue in normoxia/hypoxia and the ratio of the vessels collapsed. The *black reference lines* represent a 1:1 linear relation in tissue fraction with respect to the collapse ratio. In the stochastic and mixed scenarios, severe hypoxia did not occur until a threshold of ~15% of the vessels collapsed in the LC region. The collapse ratio threshold can be considered as a measure of LC robustness for the oxygen supply. These results illustrate how the LC vessel network can prevent severe hypoxia in the face of vessel collapses below a threshold. The threshold was not observed in systematic scenarios, where the tissue fraction of severe hypoxia exhibited a linear-like increase, closely mirroring the collapse ratio (represented by the *black solid line*). Thus, the LC robustness in the systematic collapse scenario did not prevent severe hypoxia. The fraction of tissue under normoxia could be extremely small under several conditions.

LC robustness was different for oxygenation than for blood flow. Overall LC oxygenation was more robust to distributed vessel collapses than to clustered collapses. Under the stochastic and mixed scenarios, severe hypoxia did not occur until 15% or more of the vessels had collapsed, but in the systematic scenario an LC region with severe hypoxia occurred with even a small number of collapsed vessels and increased linearly with them. This could seem at first light contradictory with the first finding above that blood perfusion decreased the slowest under the systematic scenario. The difference can be explained by the differences between the transport processes of blood and oxygen and how we determined robustness. Blood transport takes place directly within vessels, whereas oxygen transport happens both through the vessels and by diffusion within tissues. The LC vascular system is highly interconnected and dense, meaning that each of the segments that could collapse is short. This, in turn, ensures that each tissue location in the LC is supplied by multiple vessels. In the stochastic and mixed scenarios, as vessels collapse, a tissue location

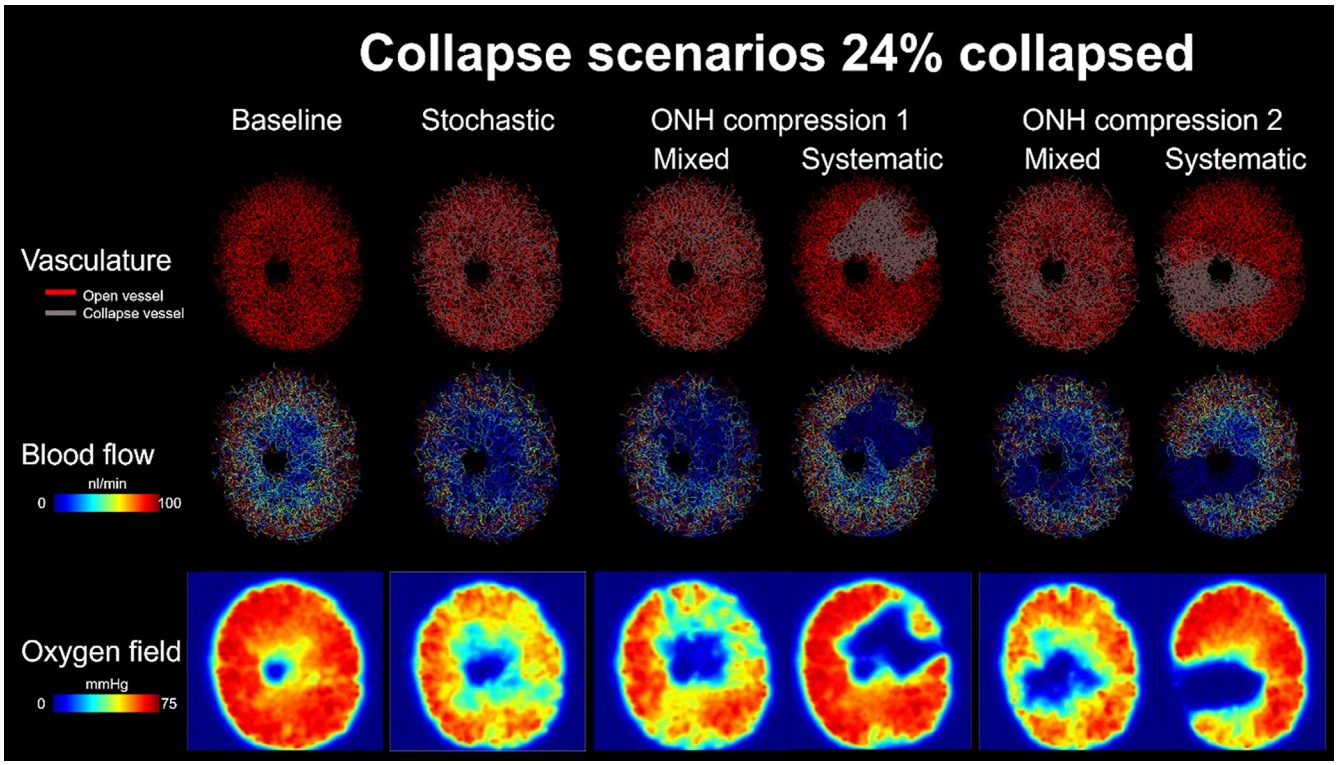

Figure 7. Vessel networks seen from the front in OD configuration. The vessel networks are colored to indicate an open or collapsed vessel segment (*top row*), or the magnitude of the blood flow (*middle row*). The *bottom row* shows the oxygen field in a cross-section through the middle of the LC. The columns correspond to the baseline condition (no collapsed vessels) and three scenarios for vessel collapse for two compression maps. These cases correspond to a collapse ratio of 24%. The systematic scenario led to clustered collapsed vessels, as would be expected from the maps of Figure 4. The collapsed vessels are more dispersed in the stochastic and mixed scenarios. Although both blood flow and oxygenation are reduced in the stochastic scenario, patterns are not obvious. For the mixed scenario, the patterns have some resemblance of the compression maps. The similarity between outcomes and with the compression map is strong for the systematic scenario. In these cases, the collapsed vessels, blood flow, and regions of low oxygen clearly colocalize with compression. This strong association explains why the tissue fraction of severe hypoxia in systematic scenarios have a near 1:1 relation to the collapse ratio, shown in Figure 6. Due to the concentration of hypoxic areas and vascular collapse in the systematic scenarios, most tissues are either normoxic or in severe hypoxia, which is also consistent with the low tissue fraction of mild hypoxia in Figure 6.

may have its oxygen supply slightly compromised, resulting in an increase in regions with mild hypoxia but avoiding severe hypoxia. It is not until the collapse ratio has increased enough to form large clusters of collapse vessels that severe hypoxia begins to occur. When this occurs there may not be much tissue left with normal oxygenation. Conversely, in the systematic scenario, vessel collapses are concentrated in the regions of large compressive deformation. This leads to a region of collapsed vessels without flow and where the closest vessels with flow are fairly distant. This causes a region of severe hypoxia locally, surrounded by a region of mild hypoxia, while most of the tissue elsewhere remains normal (or may even have higher flow and oxygenation, as discussed below).

Our findings show that, for overall blood perfusion, the LC was more robust to the clustered collapses of the systematic scenario. For overall oxygen supply, the LC was more robust to the distributed collapses of the stochastic and mixed scenarios. We believe that this difference is very important, first in terms of the kind of event that could lead to them. A local LC defect may, for example, affect oxygenation more than it affects blood perfusion. Conversely, distributed damage (say, from aging) could have a smaller impact on oxygenation but a larger impact on blood perfusion.

Blood perfusion rate has often been considered a useful clinical biomarker, likely because measures of oxygenation have been lacking. Our results emphasize that it is critical to distinguish between these two measures. Although there are good reasons sometimes to focus on blood flow by itself, if the interest is to predict or understand glaucomatous neuropathy, then oxygenation seems like the most relevant measure. The different behavior of blood perfusion and oxygenation in this study suggests that blood flow may not necessarily be the most appropriate measure.

Our results showed that locally there were small regions, or pockets, within the LC that had non-intuitive behavior in response to vessel collapses. We highlight two interesting examples: (1) pockets where blood perfusion and oxygenation increased as vessels collapsed elsewhere, and (2) pockets of normal flow surrounded by low flow. Despite the normal flow, these regions had very low oxygenation. Here, we discuss an interpretation of the findings and the mechanisms leading to them. Overall, the maps of experimentally measured IOP-induced compression, changes in blood flow, and oxygenation (Figs. 4–6, respectively) lead to the impression that there are reasonably good spatial correlations among these fields, especially in the systematic scenario. As would have been expected, vascular collapse has a negative effect on the microcirculation. The first exam-

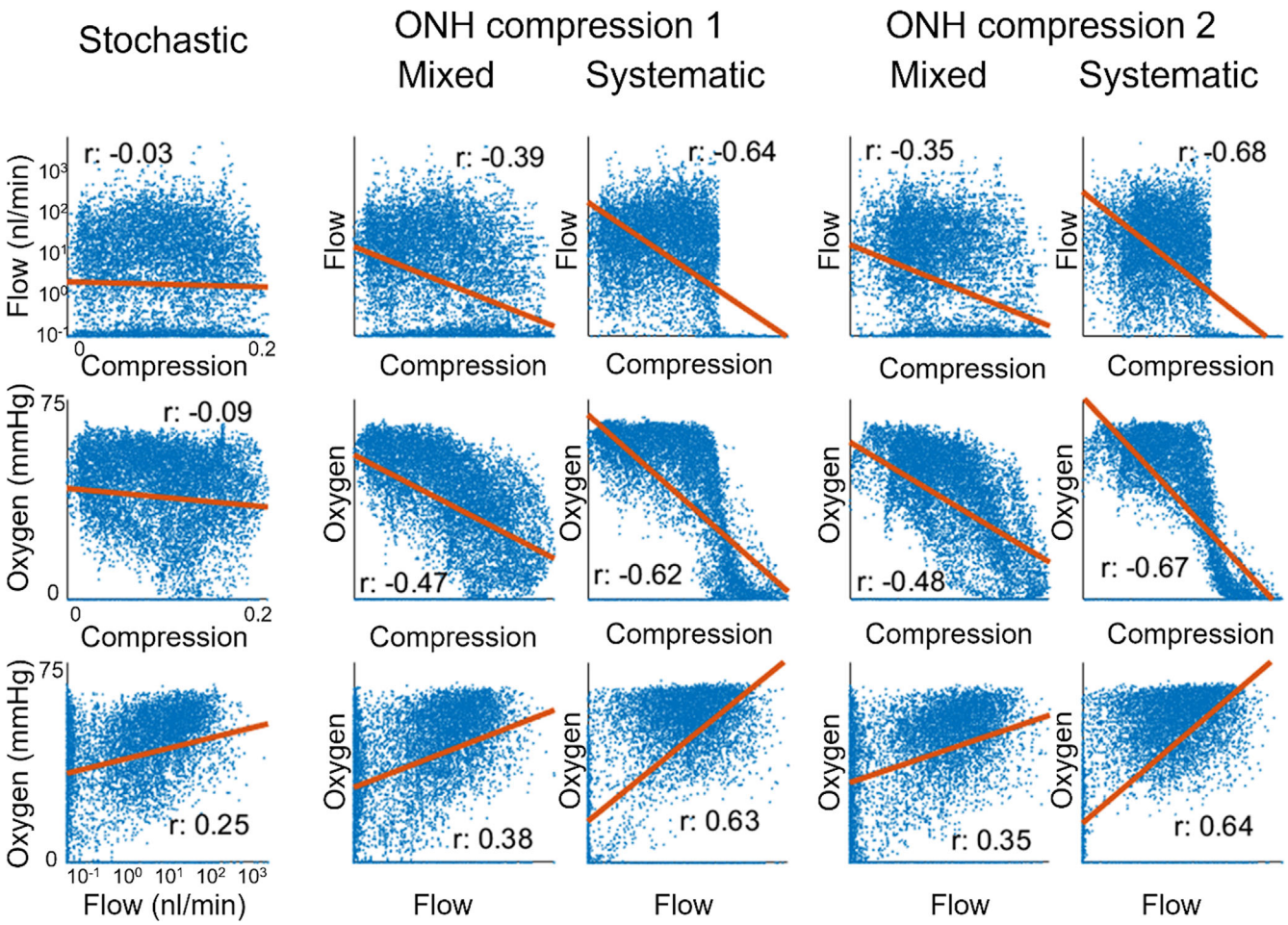

Figure 8. Scatterplots showing quantitative associations between blood flow within vessels and the compression and oxygenation surrounding the vessels (eye 1). Each *dot* represents a vessel segment, and *r* is the conventional correlation coefficient. Correlations between ONH compression and flow/oxygenation were strongest for the systematic scenario, moderate for the mixed scenario, and weakest for the stochastic scenario. For all three scenarios, there was a positive relationship between the blood flow and oxygenation. As above, the strongest correlation was observed in the systematic scenario and the weakest one in the stochastic scenario.

ple above can be understood through the examples illustrated in Figure 12. Because of the interconnected nature of the LC network, the collapse of a vessel network can lead to an increased flow elsewhere in the network. This, in turn, can result in flow and oxygenation even higher than at baseline. We can also think that, as a region of the LC becomes sufficiently blocked and thus severely hypoxic, other regions will receive flow that has "full" oxygen content. The second example—namely, islands with normal blood flow—can be understood because the LC exchanges blood with the prelaminar and laminar regions. Thus, even with many vessels collapsed a path may remain open to perfuse the region. However, despite the normal flow, the oxygen content in the blood flowing through the small region can be insufficient, resulting in the low oxygenation. This particular case can be a concern as the technology to measure oxygenation lags behind development and implementation compared with the tools to measure blood flow, such as OCTA.

We are not aware of a study on the robustness of the LC vasculature. The work here focused on physiologically relevant aspects of perfusion, such as blood flow magnitude and oxygenation. Elsewhere, studies have focused on characteristics of the network, such as connectivity and mean pathway length,[69,70] in part because these can potentially affect flow and oxygenation. By focusing on the potential effects of elevated IOP, we anticipate that this work can help us understand the risk of hypoxia and neural tissue damage in the early stages of glaucoma. In this work, we combined 3D eye-specific LC vascular networks with in vivo measured ONH compression. This allowed us to perform a more physiologically realistic hemodynamic and oxygenation simulation of the effects of elevated IOP than would be possible using a generic model. By using two vascular networks and two ONH compression maps, we were able to reduce the impact of the specific choices. Although the results were slightly different for the two vessel networks and the two experimental maps of IOP-induced compression, the trends were essentially equivalent, and the same conclusions apply to all cases.

Limitations

It is important to acknowledge the limitations of this study. An important one is that we modeled the vessel segments as either intact or collapsed, without accounting for intermedi-

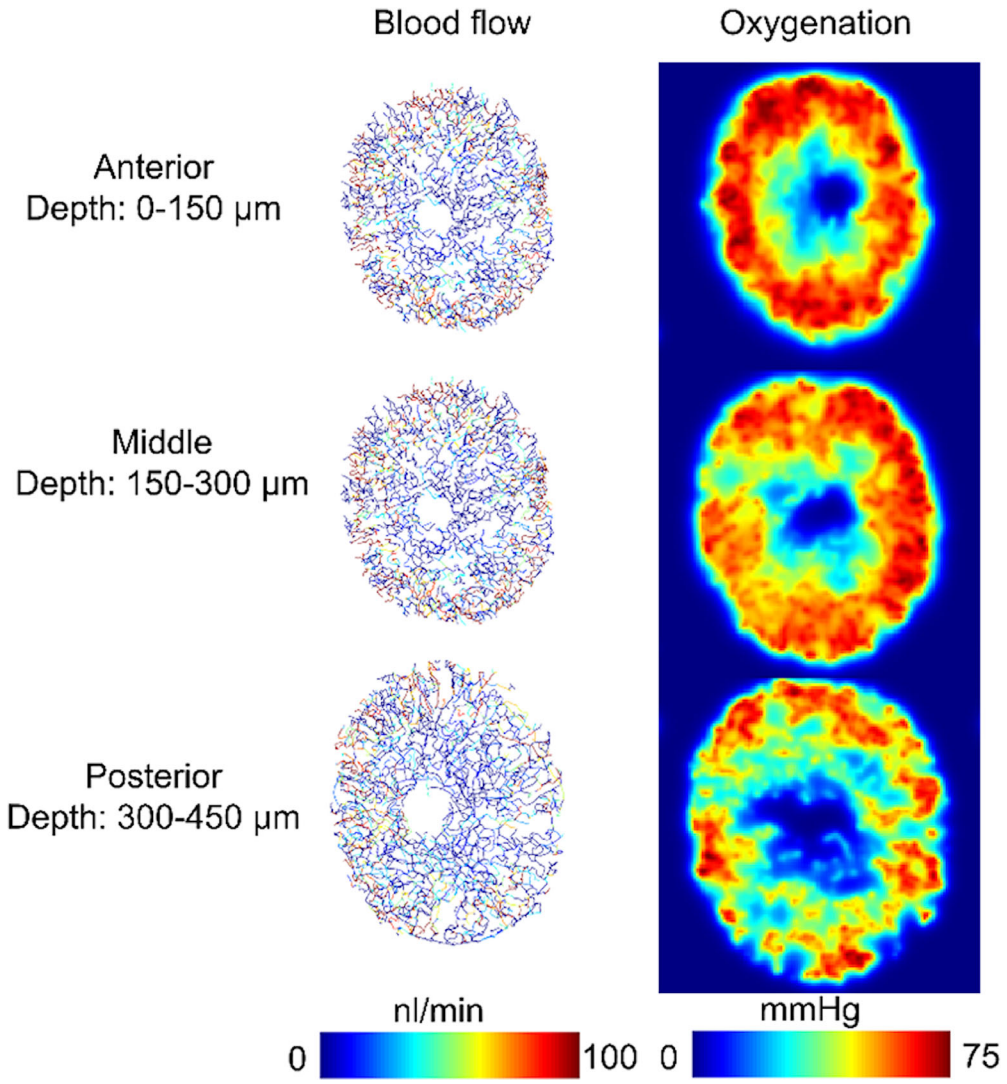

Figure 9. Baseline blood flow and oxygenation in three coronal depths of the LC of eye 1. For all planes, blood flow and oxygenation were high at the periphery and decreased toward the center.

ate states. In fact, when the surrounding tissue is deformed, blood vessels can be deformed, compressed, and twisted rather than just collapsed.[5,71] All of these events likely affect blood flow and oxygen transfer between the vessels and the adjacent tissues. The actual effects of IOP on the small-scale vessels of the LC remain unknown due to experimental limitations. This was one of the motivations for our choice to use computational models. As noted before, we are not the first to use computational models to simulate distortions of the LC vasculature. Previous work considered blood vessels as a material with the same elastic properties as the surrounding tissues.[12] Vessels, however, have different mechanical properties than the collagenous and neural tissues of the LC. Their mechanics are also potentially dependent on the lumen blood pressure. Modeling precisely IOP-related vessel distortions and their subtle effects on blood flow is certainly of interest, but non-trivial and thus out of the scope of this specific project. Herein, we considered vessel collapse as a worst-case scenario as a means to evaluate LC robustness.

It is important to note that blood pressure could influence vessel collapse. Blood flow induces shear stress along the vessel wall and exerts pressure on it. Although shear stress affects short-term autoregulation and long-term vessel remodeling, blood pressure acts perpendicular to the vessel wall, counteracting the external pressure and thereby preventing vessel collapse. If everything else remains the same, a vessel with lower blood pressure would be at a higher risk of collapse than a vessel with higher blood pressure. In our study, vessels were considered binary open/collapsed, without accounting for blood pressure effects. We acknowledge the importance of blood pressure on vessel collapse and are working to consider varying degrees of collapse based on IOP-induced compression and pressure within the vessels.

Another limitation is that the maps of IOP-related tissue compression were obtained from different eyes and not from the ones from which the reconstructions were made. It is unknown if this may have had an effect on the results. However, as noted above, the results were similar for both vessel networks and both compression maps. This suggests that the details of the vessel network do not play a key role on the effects. Nevertheless, readers should interpret

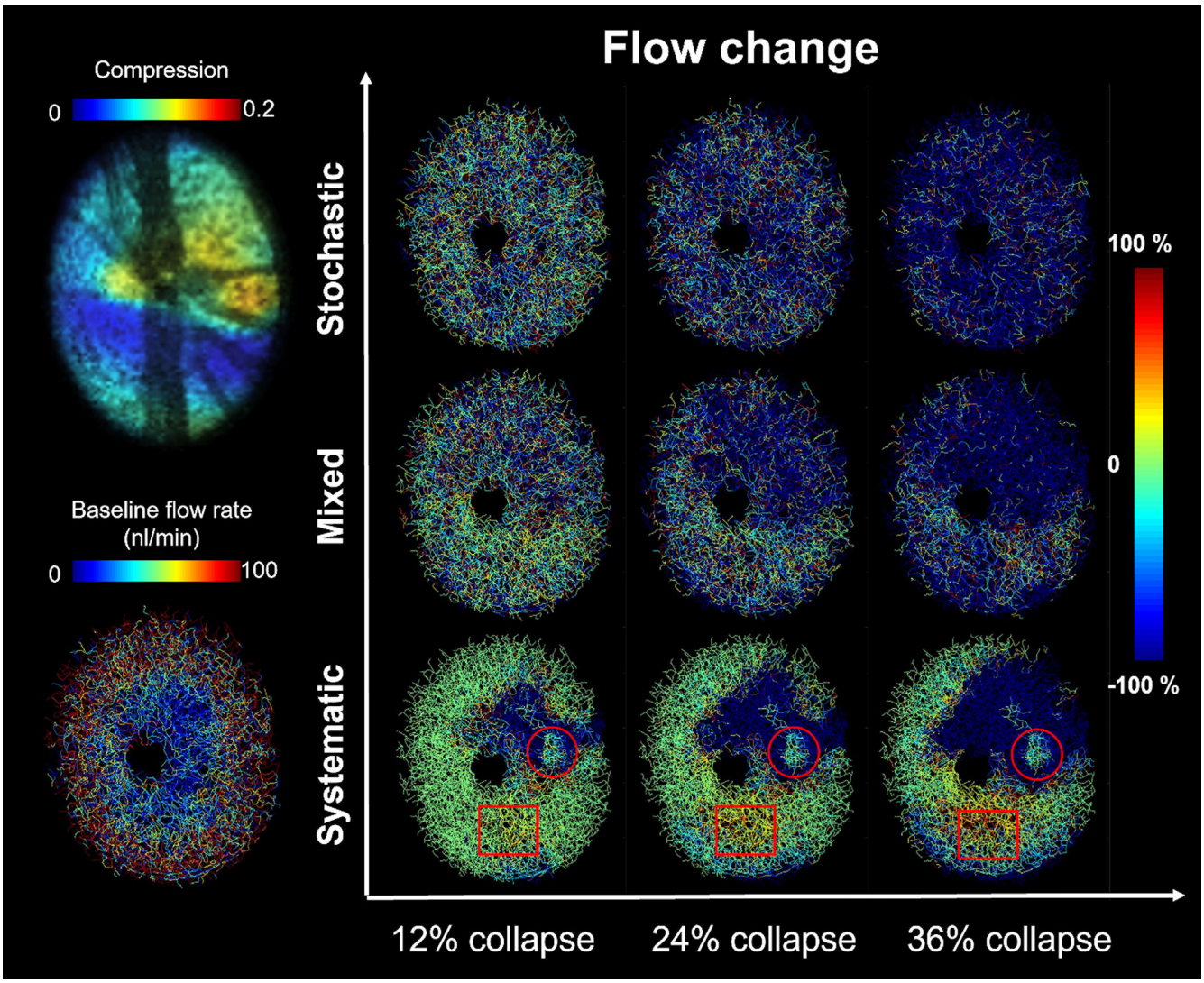

Figure 10. Maps of changes in hemodynamics for various collapse ratios. Vessels where flow did not change are indicated in *green*. In collapsed vessels, the flow was zero, and they are indicated by *deep blue*. *Yellow* and *red* indicate increased flow. Most vessels had reduced flow as the collapse ratio increased; however, for a few vessels, the blood flow increased as more vessels collapsed (*boxes*). This interesting effect is the result of vessel collapse redirecting the flow of oxygenated blood. In stochastic and mixed scenarios, this is difficult to discern because the collapsed vessels are distributed. For the systematic scenario the collapsed vessels are more concentrated, and the effect of increased oxygenation with increased collapse is more pronounced and easier to discern. Also interesting is the existence of an "island" (*circles*) of essentially normal flow surrounded by very low, but not zero, flow.

the results cautiously. Most important in this regard is that we considered only two networks and two vessel deformations that are unlikely to capture the wide range of anatomy and physiology of the ONH. It remains unclear whether the results reported herein generalize.

Our work did not consider blood flow autoregulation, a significant factor in in vivo blood supply, particularly in the eye.[55,72] Autoregulation is a regulatory mechanism that helps maintain consistent perfusion flow and oxygen supply under varying conditions.[73] Through this mechanism, tissue can regulate blood vessel radius and blood pressure, for example, in response to hypoxia signals, ensuring sufficient blood flow.[74,75] Although the precise autoregulation mechanism in LC remains unclear, we acknowledge that it could affect the LC robustness.[9,55,72,76–78] Future research should include the autoregulation effect in LC robustness analyses.

In this study, we did not consider the variation in vessel diameter and its potential impact on the robustness of the LC vasculature. To our knowledge, no literature has documented the variation of vessel diameter in the LC. Considering this, let us explore two possibilities. First, if the variation in vessel diameter is random across the LC, it could introduce an additional stochastic factor, increasing randomness in mixed and systematic scenarios, thereby aligning them closer to our stochastic scenarios. Second, if the variation in vessel diameter follows a specific spatial pattern, it seems reasonable to conjecture that vessels with smaller diameters may be more prone to collapse, resulting in lower robustness in regions with smaller diameter vessels. However, LC vessels are interconnected, and blood flow and lumen pressure within a vessel can be influenced by both upstream and downstream vessels. In addition, the type of tissue surrounding the vessels and the specific

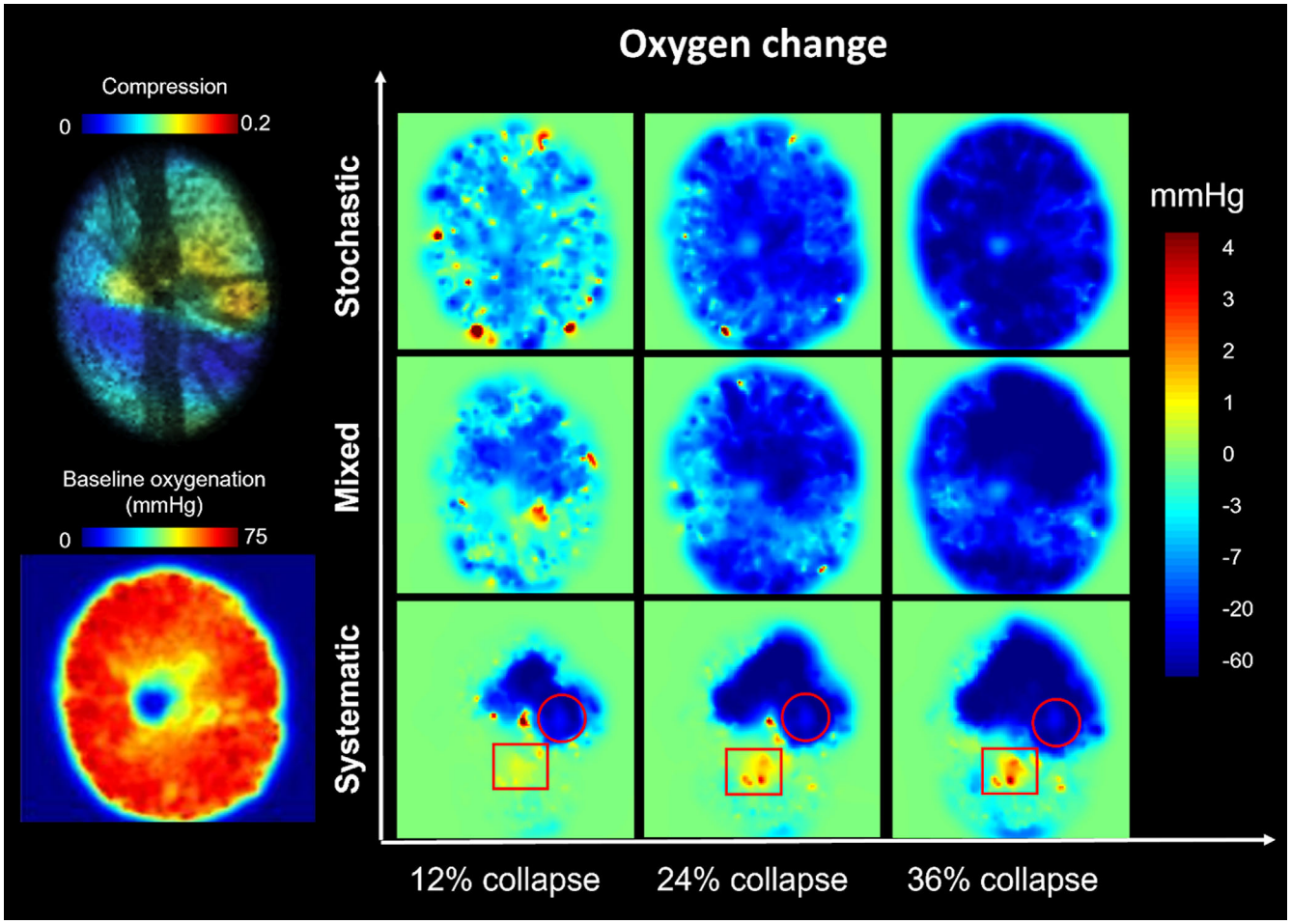

Figure 11. Changes in the oxygenation for various collapse ratios. Similar to the blood flow changes shown in Figure 10, higher collapse ratios generally led to decreased oxygenation in most of the LC, with a few areas experiencing increased oxygenation. In the systematic and mixed scenarios, a substantial collapse ratio (30%) results in a widespread decline in oxygenation across the entire LC region. However, the systematic scenarios still exhibited higher oxygenation in specific regions at higher collapse ratios. Note that the color scale is not linear, as we adjusted the colormap to enhance the visualization of regions with elevated oxygenation. The "islands" of normal flow as seen in Figure 10 (*circles*) suffered from a severe loss of oxygen.

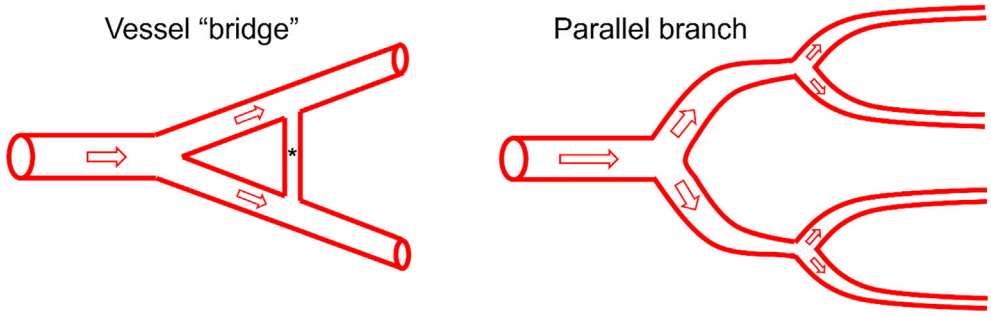

Figure 12. Two diagrams illustrating how collapsing blood vessels in one location may increase blood flow in another location. For the vessel "bridge" case on the left, because of the system symmetry, flow through the bridge vessel marked with the *asterisk* is very small. If the symmetry is disrupted by some collapsed vessels, blood flow through the bridge will increase. For the parallel branch case on the right, collapse of any branch leads to a drop of flow downstream but an increase on the alternative branches.

local biomechanical insult could be substantially different between vessels, and even within a vessel segment.[43] Consequently, the relationship between the vessel diameter and the likelihood of collapse may not be straightforward. Additional experimental evidence is needed to validate our hypothesis.

In this work, we used two fixed thresholds to distinguish among normal oxygenation, mild hypoxia, and severe

hypoxia. Although these thresholds were informed by well-supported studies, the oxygen levels that contribute to neural tissue damage remain unknown. These levels may even depend on other factors, such as age, level of neural tissue activity, and other aspects of ONH, LC, and neural tissue health, some of which are impossible to quantify. We evaluated using other thresholds, which caused the results to change slightly, but the general aspects were the same and therefore we posit that the conclusions are not tied directly to our choices. We paid closer attention to severe hypoxia as a potential lead to glaucomatous neuropathy, but chronic mild hypoxia could also trigger tissue remodeling and pathologic effects.

Consider the dynamic changes in the eye within a day (e.g., IOP spikes, saccades). The eye is adapted to minimize the risk of hypoxia at all levels of IOP, and particularly at normal IOP. However, it is challenging to maintain oxygenation at high IOP, and some patients suffer glaucoma at normal IOP, so the eye adaptation and biological design principles are complex. A brief period of hypoxia will potentially not lead to permanent tissue damage immediately. The sensitive neuronal tissue could survive about 3 minutes under severe hypoxia.[59] However, chronic hypoxia could result in chronic vessel remodeling and regulation. This is in part why we considered both mild and severe hypoxia. Further, just "survival" may not reflect damage or decreased function. We should also consider that mechanically very short IOP spikes may not actually cause as much deformation to the tissues due to the viscoelastic properties, so, for example, IOP spikes due to saccades are unlikely to lead to any substantial distortion or collapse of LC vessels. Therefore, the results from this study should be interpreted in the context of the duration of the insult and IOP variations.

Elevated IOP may affect LC blood/oxygen supply directly by distorting LC capillaries and/or indirectly by reducing perfusion through the feeding vessels, such as posterior ciliary arteries (PCAs). In this study, we only considered the direct vessel collapse effect. Based on our previous work, the arteriole and venule pressure, which drive the blood transport through the LC region, play an important role in the LC oxygenation. Therefore, we believe that the perfusion from larger feeding vessels could potentially be a major factor for LC oxygenation. However, we are not aware of conclusive evidence that either larger or smaller vessels are responsible for the loss of blood supply at elevated IOP. The potential effect of elevated IOP on the larger feeding vessel for LC region (e.g., PCAs) requires more experimental work and will be studied in the future.

In summary, we analyzed the LC vasculature robustness under various vascular collapse scenarios. The robustness of the LC vessels can help the LC area defend against some stochastic network challenges, but the LC is vulnerable to some systematic network challenges. The findings provide a systematic picture of LC robustness, including various vascular collapse mechanisms, multiple LC vascular networks, and multiple ONH compression. This is crucial for advancing our knowledge of ONH physiology and pathology.

Acknowledgments

Supported by grants from the National Institutes of Health (R01-EY023966, R01-EY031708, R01-HD083383, P30-EY008098, T32-EY017271); Eye & Ear Foundation of Pittsburgh; Research to Prevent Blindness (unrestricted grant to UPMC Ophthalmology and Stein Innovation Award to IAS); and BrightFocus Foundation.

Disclosure: **Y. Lu**, None; **Y. Hua**, None; **B. Wang**, None; **F. Zhong**, None; **A. Theophanous**, None; **S. Tahir**, None; **P.-Y. Lee**, None; **I.A. Sigal**, None

References

1. Quigley H, Anderson DR. The dynamics and location of axonal transport blockade by acute intraocular pressure elevation in primate optic nerve. *Invest Ophthalmol Vis Sci*. 1976;15:606–616.
2. Quigley HA, Nickells RW, Kerrigan LA, Pease ME, Thibault DJ, Zack DJ. Retinal ganglion cell death in experimental glaucoma and after axotomy occurs by apoptosis. *Invest Ophthalmol Vis Sci*. 1995;36:774–786.
3. Howell GR, Libby RT, Jakobs TC, et al. Axons of retinal ganglion cells are insulted in the optic nerve early in DBA/2J glaucoma. *J Cell Biol*. 2007;179:1523–1537.
4. Quigley H. Glaucoma. *Lancet*. 2011;377:1367–1377.
5. Brazile BL, Yang B, Waxman S, et al. Lamina cribrosa capillaries straighten as intraocular pressure increases. *Invest Ophthalmol Vis Sci*. 2020;61:2.
6. Hayreh S. The optic nerve head circulation in health and disease. *Ophthalmic Lit*. 1996;2:111.
7. Levitzky M, Henkind P. Angioarchitecture of the optic nerve: II. Lamina cribrosa. *Am J Ophthalmol*. 1969;68:986–996.
8. Sugiyama K, Bacon D, Morrison J, Van Buskirk E. Optic nerve head microvasculature of the rabbit eye. *Invest Ophthalmol Vis Sci*. 1992;33:2251–2261.
9. Mackenzie PJ, Cioffi GA. Vascular anatomy of the optic nerve head. *Can J Ophthalmol*. 2008;43:308–312.
10. Burgoyne CF, Downs JC, Bellezza AJ, Suh J-KF, Hart RT. The optic nerve head as a biomechanical structure: a new paradigm for understanding the role of IOP-related stress and strain in the pathophysiology of glaucomatous optic nerve head damage. *Prog Retin Eye Res*. 2005;24:39–73.
11. Chuangsuwanich T, Birgersson KE, Thiery A, Thakku SG, Leo HL, Girard MJ. Factors influencing lamina cribrosa microcapillary hemodynamics and oxygen concentrations. *Invest Ophthalmol Vis Sci*. 2016;57:6167–6179.
12. Chuangsuwanich T, Hung PT, Wang X, et al. Morphometric, hemodynamic, and biomechanical factors influencing blood flow and oxygen concentration in the human lamina cribrosa. *Invest Ophthalmol Vis Sci*. 2020;61:3.
13. Sigal IA, Ethier CR. Biomechanics of the optic nerve head. *Exp Eye Res*. 2009;88:799–807.
14. Sigal IA, Flanagan JG, Tertinegg I, Ethier CR. Predicted extension, compression and shearing of optic nerve head tissues. *Exp Eye Res*. 2007;85:312–322.
15. Sigal IA, Grimm JL. A few good responses: which mechanical effects of IOP on the ONH to study? *Invest Ophthalmol Vis Sci*. 2012;53:4270–4278.
16. Stefánsson E, Pedersen DB, Jensen PK, et al. Optic nerve oxygenation. *Prog Retin Eye Res*. 2005;24:307–332.
17. Krzyżanowska-Berkowska P, Czajor K, Iskander DR. Associating the biomarkers of ocular blood flow with lamina cribrosa parameters in normotensive glaucoma suspects. Comparison to glaucoma patients and healthy controls. *PLoS One*. 2021;16:e0248851.
18. Hamasaki D, Fujino T. Effect of intraocular pressure on ocular vessels: filling with India ink. *Arch Ophthalmol*. 1967;78:369–379.
19. Panda SK, Cheong H, Tun TA, et al. The three-dimensional structural configuration of the central retinal vessel trunk and branches as a glaucoma biomarker. *Am J Ophthalmol*. 2022;240:205–216.

Investigative Ophthalmology & Visual Science

20. Carichino L, Guidoboni G, Arieli Y, Siesky BA, Harris A. Effect of lamina cribrosa deformation on the hemodynamics of the central retinal artery: a mathematical model. *Invest Ophthalmol Vis Sci*. 2012;53:2836.
21. Fechtner RD, Weinreb RN. Mechanisms of optic nerve damage in primary open angle glaucoma. *Surv Ophthalmol*. 1994;39:23–42.
22. Quigley HA, McKinnon SJ, Zack DJ, et al. Retrograde axonal transport of BDNF in retinal ganglion cells is blocked by acute IOP elevation in rats. *Invest Ophthalmol Vis Sci*. 2000;41:3460–3466.
23. Brooks D, Samuelson D, Gelatt K. Ultrastructural changes in laminar optic nerve capillaries of beagles with primary open-angle glaucoma. *Am J Vet Res*. 1989;50:929–935.
24. Geijer C, Bill A. Effects of raised intraocular pressure on retinal, prelaminar, laminar, and retrolaminar optic nerve blood flow in monkeys. *Invest Ophthalmol Vis Sci*. 1979;18:1030–1042.
25. Beach J, Ning J, Khoobehi B. Oxygen saturation in optic nerve head structures by hyperspectral image analysis. *Curr Eye Res*. 2007;32:161–170.
26. Carreau A, Hafny-Rahbi BE, Matejuk A, Grillon C, Kieda C. Why is the partial oxygen pressure of human tissues a crucial parameter? Small molecules and hypoxia. *J Cell Mol Med*. 2011;15:1239–1253.
27. Ferrez P, Chamot S, Petrig B, Pournaras C, Riva C. Effect of visual stimulation on blood oxygenation in the optic nerve head of miniature pigs: a pilot study. *Klin Monbl Augenheilkd*. 2004;221:364–366.
28. Ortiz-Prado E, Dunn JF, Vasconez J, Castillo D, Viscor G. Partial pressure of oxygen in the human body: a general review. *Am J Blood Res*. 2019;9:1.
29. McKeown S. Defining normoxia, physoxia and hypoxia in tumours—implications for treatment response. *Br J Radiol*. 2014;87:20130676.
30. Davies AL, Desai RA, Bloomfield PS, et al. Neurological deficits caused by tissue hypoxia in neuroinflammatory disease. *Ann Neurol*. 2013;74:815–825.
31. Rao HL, Pradhan ZS, Weinreb RN, et al. A comparison of the diagnostic ability of vessel density and structural measurements of optical coherence tomography in primary open angle glaucoma. *PLoS One*. 2017;12:e0173930.
32. Mari JM, Strouthidis NG, Park SC, Girard MJ. Enhancement of lamina cribrosa visibility in optical coherence tomography images using adaptive compensation. *Invest Ophthalmol Vis Sci*. 2013;54:2238–2247.
33. Pi S, Hormel TT, Wei X, et al. Retinal capillary oximetry with visible light optical coherence tomography. *Proc Natl Acad Sci USA*. 2020;117:11658–11666.
34. Numa S, Akagi T, Uji A, et al. Visualization of the lamina cribrosa microvasculature in normal and glaucomatous eyes: a swept-source optical coherence tomography angiography study. *J Glaucoma*. 2018;27:1032–1035.
35. Sigal IA, Wang B, Strouthidis NG, Akagi T, Girard MJ. Recent advances in OCT imaging of the lamina cribrosa. *Br J Ophthalmol*. 2014;98:ii34–ii39.
36. Qian X, Kang H, Li R, et al. In vivo visualization of eye vasculature using super-resolution ultrasound microvessel imaging. *IEEE Trans Biomed Eng*. 2020;67:2870–2880.
37. Li Y, Cheng H, Duong TQ. Blood-flow magnetic resonance imaging of the retina. *NeuroImage*. 2008;39:1744–1751.
38. Sugiyama T, Araie M, Riva CE, Schmetterer L, Orgul S. Use of laser speckle flowgraphy in ocular blood flow research. *Acta Ophthalmol*. 2010;88:723–729.
39. Causin P, Guidoboni G, Harris A, Prada D, Sacco R, Terragni S. A poroelastic model for the perfusion of the lamina cribrosa in the optic nerve head. *Math Biosci*. 2014;257:33–41.
40. Lee P-Y, Hua Y, Brazile BL, Yang B, Wang L, Sigal IA. A workflow for three-dimensional reconstruction and quantification of the monkey optic nerve head vascular network. *J Biomech Eng*. 2022;144:061006.
41. Hua Y, Lu Y, Walker J, et al. Eye-specific 3D modeling of factors influencing oxygen concentration in the lamina cribrosa. *Exp Eye Res*. 2022;220:109105.
42. Lu Y, Hu D, Ying W. A fast numerical method for oxygen supply in tissue with complex blood vessel network. *PLoS One*. 2021;16:e0247641.
43. Waxman S, Brazile BL, Yang B, et al. Lamina cribrosa vessel and collagen beam networks are distinct. *Exp Eye Res*. 2022;215:108916.
44. An D, Pulford R, Morgan WH, Yu D-Y, Balaratnasingam C. Associations between capillary diameter, capillary density, and microaneurysms in diabetic retinopathy: a high-resolution confocal microscopy study. *Transl Vis Sci Technol*. 2021;10:6.
45. Secomb TW, Hsu R, Park EY, Dewhirst MW. Green's function methods for analysis of oxygen delivery to tissue by microvascular networks. *Ann Biomed Eng*. 2004;32:1519–1529.
46. Hayreh SS, Zimmerman MB, Beri M, Podhajsky P. Intraocular pressure abnormalities associated with central and hemicentral retinal vein occlusion. *Ophthalmology*, 2004;111:133–141.
47. Tran H, Wallace J, Zhu Z, et al. Seeing the hidden lamina: effects of exsanguination on the optic nerve head. *Invest Ophthalmol Vis Sci*. 2018;59:2564–2575.
48. Sigal IA, Grimm JL, Jan N-J, Reid K, Minckler DS, Brown DJ. Eye-specific IOP-induced displacements and deformations of human lamina cribrosa. *Invest Ophthalmol Vis Sci*. 2014;55:1–15.
49. Tran H, Wallace J, Voorhees AP, et al. Lamina cribrosa shape is different between humans and monkeys at baseline IOP and is changed differently with IOP elevations. *Invest Ophthalmol Vis Sci*. 2017;58:3157.
50. Nitta F, Kunikata H, Aizawa N, et al. The effect of intravitreal bevacizumab on ocular blood flow in diabetic retinopathy and branch retinal vein occlusion as measured by laser speckle flowgraphy. *Clin Ophthalmol*. 2014;8:1119–1127.
51. Ghassemi F, Berijani S, Roohipoor R, et al. Vascular density of optic nerve head in diabetic retinopathy using optical coherence tomography angiography. *Int J Retina Vitreous*. 2020;6:62.
52. Milanovic S, Shaw K, Hall C, Payne S. Investigating the role of pericytes in cerebral autoregulation: a modeling study. *Physiol Meas*. 2021;42:054003.
53. Wang L, Cull GA, Fortune B. Optic nerve head blood flow response to reduced ocular perfusion pressure by alteration of either the blood pressure or intraocular pressure. *Curr Eye Res*. 2015;40:359–367.
54. Liang Y, Fortune B, Cull G, Cioffi GA, Wang L. Quantification of dynamic blood flow autoregulation in optic nerve head of rhesus monkeys. *Exp Eye Res*. 2010;90:203–209.
55. Wang L, Burgoyne CF, Cull G, Thompson S, Fortune B. Static blood flow autoregulation in the optic nerve head in normal and experimental glaucoma. *Invest Ophthalmol Vis Sci*. 2014;55:873–880.
56. Shilo M, Gefen A. Identification of capillary blood pressure levels at which capillary collapse is likely in a tissue subjected to large compressive and shear deformations. *Comput Methods Biomech Biomed Engin*. 2012;15:59–71.
57. Zhong F, Wang B, Wei J, et al. A high-accuracy and high-efficiency digital volume correlation method to characterize in-vivo optic nerve head biomechanics from optical coherence tomography. *Acta Biomater*. 2022;143:72–86.

Investigative Ophthalmology & Visual Science

58. Chen C-L, Bojikian KD, Gupta D, et al. Optic nerve head perfusion in normal eyes and eyes with glaucoma using optical coherence tomography-based microangiography. *Quant Imaging Med Surg*. 2016;6:125–133.
59. Leach R, Treacher D. Oxygen transport-2. Tissue hypoxia. *BMJ*. 1998;317:1370–1373.
60. Loiacono LA, Shapiro DS. Detection of hypoxia at the cellular level. *Crit Care Clin*. 2010;26:409–421.
61. De Filippis L, Delia D. Hypoxia in the regulation of neural stem cells. *Cell Mol Life Sci*. 2011;68:2831–2844.
62. Erecińska M, Silver IA. Tissue oxygen tension and brain sensitivity to hypoxia. *Respir Physiol*. 2001;128:263–276.
63. Hockel M, Vaupel P. Tumor hypoxia: definitions and current clinical, biologic, and molecular aspects. *J Natl Cancer Inst*. 2001;93:266–276.
64. Pries AR, Secomb TW. *Microcirculation*. Amsterdam: Elsevier; 2008:3–36.
65. Boltz A, Schmidl D, Werkmeister RM, et al. Regulation of optic nerve head blood flow during combined changes in intraocular pressure and arterial blood pressure. *J Cereb Blood Flow Metab*. 2013;33:1850–1856.
66. Iwase T, Akahori T, Yamamoto K, Ra E, Terasaki H. Evaluation of optic nerve head blood flow in response to increase of intraocular pressure. *Sci Rep*. 2018;8:17235.
67. Kiyota N, Shiga Y, Ichinohasama K, et al. The impact of intraocular pressure elevation on optic nerve head and choroidal blood flow. *Invest Ophthalmol Vis Sci*. 2018;59:3488–3496.
68. Qian X, Huang C, Li R, et al. Super-resolution ultrasound localization microscopy for visualization of the ocular blood flow. *IEEE Trans Biomed Eng*. 2021;69:1585–1594.
69. Papadopoulos L, Blinder P, Ronellenfitsch H, et al. Comparing two classes of biological distribution systems using network analysis. *PLoS Comput Biol*. 2018;14:e1006428.
70. Tero A, Takagi S, Saigusa T, et al. Rules for biologically inspired adaptive network design. *Science*. 2010;327:439–442.
71. Bullitt E, Zeng D, Gerig G, et al. Vessel tortuosity and brain tumor malignancy: a blinded study1. *Acad Radiol*. 2005;12:1232–1240.
72. Yu J, Liang Y, Thompson S, Cull G, Wang L. Parametric transfer function analysis and modeling of blood flow autoregulation in the optic nerve head. *Int J Physiol Pathophysiol Pharmacol*. 2014;6:13–22.
73. Riva CE, Hero M, Titze P, Petrig B. Autoregulation of human optic nerve head blood flow in response to acute changes in ocular perfusion pressure. *Graefes Arch Clin Exp Ophthalmol*. 1997;235:618–626.
74. Greisen G. Autoregulation of cerebral blood flow in newborn babies. *Early Hum Dev*. 2005;81:423–428.
75. Fallon T, Maxwell D, Kohner E. Retinal vascular autoregulation in conditions of hyperoxia and hypoxia using the blue field entoptic phenomenon. *Ophthalmology*. 1985;92:701–705.
76. Hayreh SS. Blood flow in the optic nerve head and factors that may influence it. *Prog Retin Eye Res*. 2001;20:595–624.
77. Orgül S, Gugleta K, Flammer J. Physiology of perfusion as it relates to the optic nerve head. *Surv Ophthalmol*. 1999;43:S17–S26.
78. Mozaffarieh M, Grieshaber MC, Flammer J. Oxygen and blood flow: players in the pathogenesis of glaucoma. *Mol Vis*. 2008;14:224.

Appendix

Systematic Collapse Scenario

The blood vessels collapse in a certain order of the magnitude of strain value. Specifically, the blood vessels collapse in series, starting with vessels experiencing the highest magnitude of surrounding tissue compression followed by the vessels with the second largest compression and so forth. The collapse process repeats until the proportion of collapsed vessel reaches our setting for R_c.

Therefore, for a given collapse ratio R_c, the collapse probability (C_v) for each vessel is,

$$c_v = \begin{cases} 1, & \varepsilon_v \geq \varepsilon_{v_{Rc}} \\ 0, & \varepsilon_v < \varepsilon_{v_{Rc}} \end{cases}$$

where $\varepsilon_{v_{Rc}}$ is the R_cth largest value in all of the vessel compression values.

Stochastic Collapse Scenario

The blood vessels collapse based on a uniform likelihood. The collapse probability (C_v) for each vessel is a uniform constant equal to the collapse ratio,

$$C_v = R_c.$$

Mixed Collapse Scenario

The blood vessels collapse based on a weighted likelihood. The collapse probability (C_v) for each vessel is proportional to the strain value (especially the compression value) at that location,

$$C_v = \rho \varepsilon_v R_c$$

$$\rho = \frac{1}{\sum_i \varepsilon_{v_i}}$$

where ε_v is the average tissue compression at the surface of the vessel, and ρ is the normalization factor.